Polymer Testing 125 (2023) 108109

Contents lists available at ScienceDirect

Polymer Testing

journal homepage: www.elsevier.com/locate/polytest

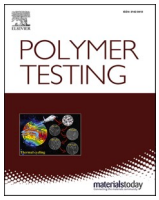

Injectable EC-BMSC hydrogel with prolonged VEGF action for enhanced angiogenesis

Shuqin Chen [a,1], Bing Han [a,1], Yanran Zhao [b], Yingying Ren [b], Shili Ai [b], Moran Jin [a], Yilin Song [a], Xiaozhong Qu [b,**], Xiaoyan Wang [a,*]

[a] Department of Cariology and Endodontology, Peking University School and Hospital of Stomatology, National Clinical Research Center for Oral Diseases, National Engineering Laboratory for Digital and Material Technology of Stomatology, Beijing Key Laboratory of Digital Stomatology, Beijing, China
[b] College of Materials Science and Opto-electronic Technology, University of Chinese Academy of Sciences, Beijing, China

ARTICLE INFO

Keywords:
Early enhanced angiogenesis
EC-BMSC co-culture
Vascular endothelial growth factor
Dynamic multi-crosslinked hydrogel
Vascularized tissue engineering

ABSTRACT

Tissue regeneration necessitates rapid and mature angiogenesis, while insufficient vascularization along with tissue implantation hinders the great potential applications. Endothelial cells (ECs) and bone marrow mesenchymal cells (BMSCs) are responsible for the angiogenesis in preparing bone tissue. Herein, we proposed the realization of the angiogenesis by co-culturing ECs and BMSCs within an injectable multi-crosslinked double-network (DN) hydrogel, composed of glycol chitosan (GC)/benzaldehyde-capped poly (ethylene oxide) (OHC-PEO-CHO) and calcium alginate (Alg). The hydrogel is crosslinked by dynamic interplay allowing the encapsulation, migration and proliferation of the cells. The hydrogel is capable to carry vascular endothelial growth factor (VEGF) with prolonging action within the matrix to effectively regulate the cell behavior. Co-existence of ECs and BMSCs with the VEGF within the hydrogel-based extracellular matrix (ECM) plays a key role in mediating the formation of a mature vascular structure with endothelium and pericyte. The neovascularization is closely related with the VEGF/VEGFR2/ERK signaling pathway. The finding indicates the direction toward future vascularized tissue regeneration by using a hydrogel-based scaffold with adjustable microenvironment by incorporation of functional growth factors.

1. Introduction

Tissue engineering (TE) is promising to construct tissues and organs for clinical treatments of the defects and damages. Early formation of three-dimensional (3D) vascular network plays a key role in ensuring adequate supplement of nutrients and oxygen as well as effective removal of waste products. Although TE has achieved great progresses, insufficient vascularization caused by tissue implantation becomes a great hindrance in further exploring the clinical applications [1–3].

It is important to develop methods for the effective construction of rapid, stable and mature angiogenesis in tissue regeneration [4–6]. Introduction of angiogenic growth factors (GFs) within the 3D scaffolds is proven effective to promote angiogenesis, which is universal for many GFs covering vascular endothelial growth factor (VEGF), platelet-derived growth factor (PDGF), angiopoietin-2 (Ang-2), and fibroblast growth factor-2 (FGF-2). Among the GFs, VEGF is capable to directly activate the downstream signaling pathway in vascular endothelial cells upon combination with the vascular endothelial growth factor receptor 2 (VEGFR2). VEGF, as the most important GF for inducing angiogenesis, has been extensively employed to regulate the vessel formation and vascularized TE [6]. It is crucial to acquire a sufficiently high concentration of VEGF for a sufficient action time [7]. TE to carry VEGF with scaffolds has proven effective to prolong the action of VEGF for stable angiogenesis [8,9]. Hydrogel as an ideal 3D scaffold is advantageous in TE owing to the excellent biocompatibility, high water content, tunable mechanic and physicochemical performances, and compartmentalization of cells [10–12]. Chen et al. [13] reported the formation of a microvascular network by using a GelMA hydrogel. Li et al. [14] reported using an injectable hydrogel to carry micro-RNA with a significantly enhanced angiogenesis for myocardial infarction therapy.

Mature vessels should contain endothelial cells binding at the inner

* Corresponding author.
** Corresponding author.
E-mail addresses: quxz@iccas.ac.cn (X. Qu), wangxiaoyan@pkuss.bjmu.edu.cn (X. Wang).
[1] Shuqin Chen and Bing Han contributed equally to this work.

https://doi.org/10.1016/j.polymertesting.2023.108109
Received 5 June 2023; Received in revised form 11 June 2023; Accepted 12 June 2023
Available online 21 June 2023

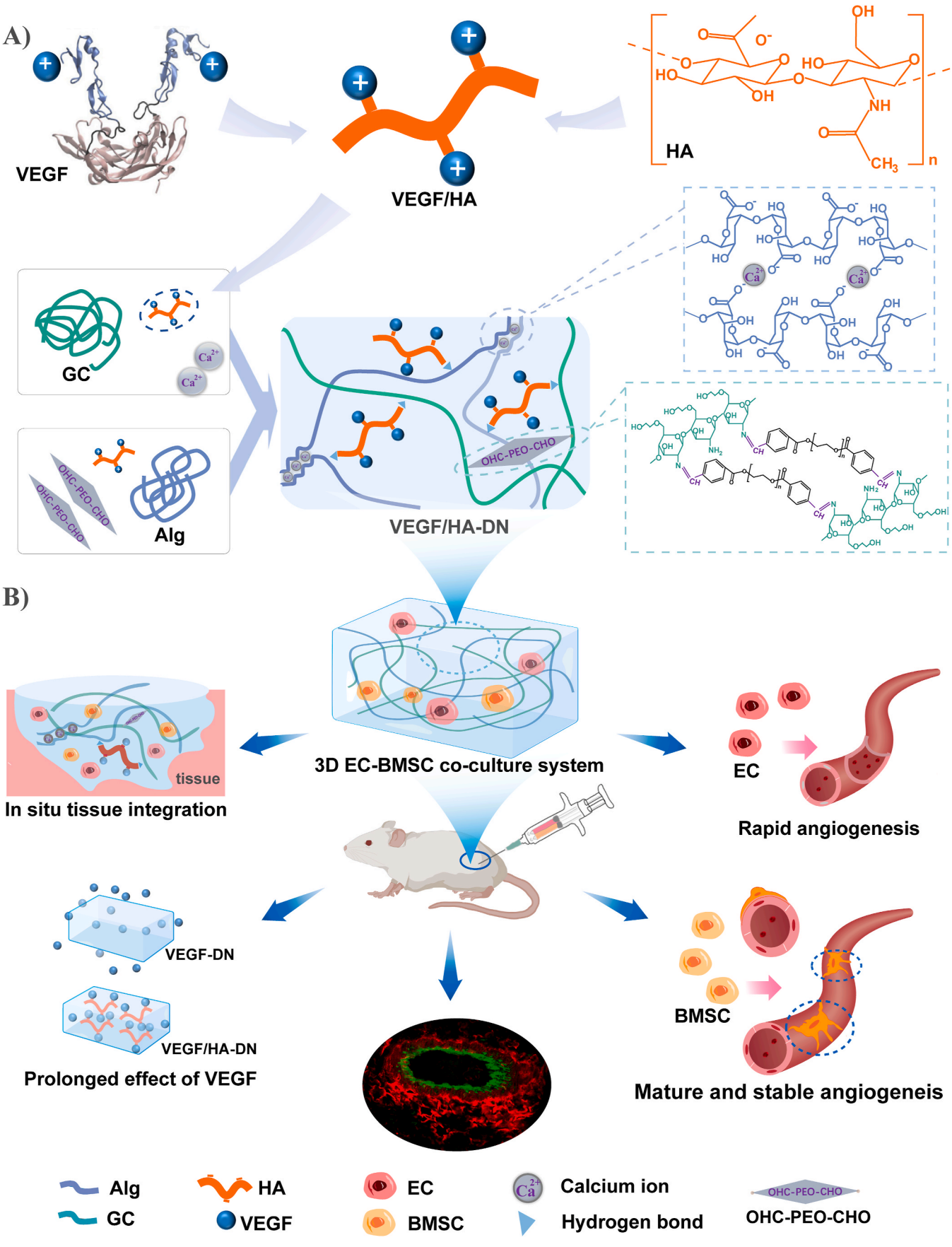

(caption on next page)

Scheme 1. Synthesis of the VEGF/HA-DN hydrogel toward angiogenesis. (A) VEGF connection with the negatively charged HA via electrostatic interaction forms the VEGF/HA complex. Preparation of the DN hydrogel via dynamic crosslinking by Schiff base reaction and ionic interaction. Dibenzaldehyde-capped poly (ethylene oxide) (OHC-PEO-CHO) and GC form the first network, while sodium alginate (Alg) and calcium chloride ($CaCl_2$) form the second network. In order to achieve a prolonging effect of VEGF, inclusion of HA allows the stable entrapping of VEGF within the DN hydrogel via forming the VEGF/HA complex. Connection of VEGF/HA within the DN hydrogel via calcium ion bridging and hydrogen bonding forms the VEGF/HA-DN hydrogel. The structure of VEGF is drawn accordingly [37]. (B) Biological properties of the VEGF/HA-DN hydrogel, including injectability, tissue integration, and prolonged effect of VEGF. As a 3D EC-BMSC co-culture scaffold, these features of the VEGF/HA-DN hydrogel are beneficial to rapid, stable and mature angiogenesis.

wall and the covered pericytes which are important for functional angiogenesis. Lack of pericytes is related with the diseases such as vascular malformations, stroke, diabetic retinopathy and cancer [15]. Although cell-based strategies of endothelial cells (ECs) have been proposed in recent years, formation of mature and functional vessels remains challenging. In the formation of vascular networks by ECs, effective recruitment of host pericytes is difficult, leading to a very long recruitment process *in vivo*. In order to overcome difficult isolation of pericytes, other functional cell types should become alternatives. Co-delivery of EC-human bone marrow-derived mesenchymal stem cell (EC-BMSC) and EC-human adipose-derived stem cell (EC-ADSC) has proven effective to form functional capillary networks [16]. Bone marrow mesenchymal stem cells (BMSCs) as the most common mesenchymal stem cells (MSCs) are effective to promote the differentiation of endothelial progenitor cells (EPCs) toward mature EC phenotypes and the overall stabilization of blood vessels [17]. It is anticipated that co-culture of ECs and BMSCs within 3D scaffolds would provide a robust method to construct the early functional vessels.

Herein, we propose using an injectable dynamically crosslinked hydrogel as a 3D extracellular matrix (ECM) to co-culture EC-BMSC in the presence of VEGF to construct an early, stable and mature 3D vascular network (Scheme 1). The injectable hydrogel is composed of a glycol chitosan (GC)/benzaldehyde-capped poly (ethylene oxide) (OHC-PEO-CHO) and calcium alginate (Alg), which are responsible for the benzoic-imine covalent dynamic bonding and electrostatic interaction to form the robust hydrogel [18]. The dynamic crosslinking within the hydrogel drives the gelation [19], enabling the encapsulation and proliferation of living cells under mild conditions [20]. In order to achieve a prolonging effect of VEGF, hyaluronic acid (HA) is introduced to the GC/Alg double-network (DN) hydrogel forming a multi-crosslinked structure in the hydrogel matrix via ionic and hydrogen binding, while the interaction of VEGF is adjusted by electrostatic coupling to gain a long-term activity in the scaffold. The resultant 3D EC-BMSC co-culture system with a prolonging VEGF action enables the angiogenesis rapid, stable and mature.

2. Methods & materials

2.1. Materials

Poly (ethylene oxide) (PEO, MW = 2 kDa) and Alg (W201502) were purchased from Sigma-Aldrich (St. Louis, USA). GC (G810700) was purchased from Macklin (Shanghai, China). $CaCl_2$ was purchased from Solarbio (Beijing, China). HA (H832247) was purchased from Meryer (Shanghai, China). OHC-PEO-CHO was synthesized accordingly [21,22]. Recombinant human VEGF was obtained from Proteintech (Wuhan, China).

2.2. Preparation of the injectable multi-crosslinked DN hydrogels

The dispersion of VEGF/HA was prepared by mixing 20 μL of VEGF solution (50 μg/mL) in 2 mL of HA solution (2.5% w/t) under ultrasonic vibration for 3 min. Two mixtures of GC (4% w/t) and $CaCl_2$ (1% w/t), Alg (2% w/t) and OHC-PEO-CHO (1% w/t) were prepared. The dispersion of VEGF/HA was fed to each mixture at a volume ratio of 1:9 to achieve the corresponding mixtures containing VEGF. After the two VEGF contained mixtures were packaged in a dual-syringe kit and injected in a mold, a multi-crosslinked DN hydrogel (named as VEGF/HA-DN) formed by standing for 0.5 h to ensure a complete gelation. Concentration of VEGF in the hydrogel was measured as 50 ng/mL. Three hydrogels of VEGF-DN (without HA), HA-DN (without VEGF), and DN (without HA and VEGF) were prepared as comparative ones.

2.3. Characterization of the injectable hydrogel scaffolds

Scanning electron microscope (SEM) (JSM-7900F, JEOL) was used to observe the microscopic structure of the hydrogels. Prior to SEM, the samples were vacuum lyophilized, sliced, placed on the conductive gel and sputtered with gold for SEM observation.

Cylindrical hydrogel samples with a height of 10 mm and a diameter of 10 mm were fabricated for the measurement using a universal testing machine (Instron, MA, USA). The load was set at 100 N with a rate at 1 mm/min for the compressive test.

In the determination of swelling ratio, the samples were freeze-dried and placed in the phosphate-buffered saline (PBS) of 2 mL at 37 °C. Weight of the hydrogel was measured after swelling for various times to calculate the swelling ratio by the weight increment to the original weight. The samples were soaked in ultra-pure water at 37 °C for various times to measure the degradation ratio by the weight loss to the original weight.

Freeze-dried powder samples were mixed with IR-grade potassium bromide. Each mixture was dried and packed for the Fourier transform infrared (FT-IR) spectroscopy characterization on Thermo Scientific Nicolet iS50 with a resolution of 1 cm^{-1}.

Dynamic light scattering measurements of the VEGF (50 μg/mL), VEGF/HA (0.5% w/t) and HA (0.5% w/t) solutions were performed on Malvern Zetasizer (Nano ZS).

The samples of VEGF/HA, VEGF-DN hydrogel and VEGF/HA-DN hydrogel were placed in a dialysis membrane with a pore size of 45 nm for the accumulative release analysis. The dialysis membranes were placed in 15 mL centrifuge tubes with 5 mL of ultra-pure water. The tubes were placed in a shaker at 37 °C and a speed of 200 rpm. After different intervals, 1 mL of solution was sampled from the tube and stored at −20 °C. After each sampling, 1 mL of ultra-pure water was supplemented to the centrifuge tube. Determination of VEGF concentration in each sample was conducted using the Authentkine™ Human VEGF ELISA kit (Proteintech, Wuhan, China).

A hydrogel of 0.2 mL was injected at the 25-mm diameter disc sample area of the rheometer (HAAKE MARS; Thermo Fisher Scientific, Waltham, MA) for the rheological characterization. The linear viscoelastic regions in the strain scanning and frequency scanning were determined at 37 °C. A hydrogel of 0.5 mL was injected through a dual-syringe kit vertically at a fixed site with a slope of 30° to determine a flowable time when the hydrogel stopped flowing.

2.4. In vitro observation of 3D EC-BMSC co-culture in the hydrogels

2.4.1. Cellular morphology of 3D EC-BMSC co-culture in the hydrogels in vitro

Human vascular endothelial cell (EA.hy926) was purchased from the Shanghai Cell Bank of the Chinese Academy of Sciences, and cultured in Dulbecco's modified Eagle's medium (DMEM) (Invitrogen, USA) with 10% of fetal bovine serum (FBS) (Ausgene, Australia) and 1% of penicillin/streptomycin (Invitrogen, USA). Human bone marrow mesenchymal stem cell (BMSCs) was purchased (Procell, Wuhan, China) and cultured in the complete mesenchymal stem cell medium (MSCM)

(Sciencell, USA) with 5% of FBS, 1% of Mesenchymal Stem Cell Growth Supplement (MSCGS) and 1% of penicillin/streptomycin. The cells were cultured in a CO_2 incubator at 37 °C, and sub-cultured at 80–90% confluence.

The solutions of GC (4% w/t), OHC-PEO-CHO (1% w/t), Alg (2% w/t) and $CaCl_2$ (1% w/t) were prepared by using a serum-free combined medium (DMEM/MSCM ratio of 1:1). A suspension consisting of EA. hy926 (2×10^7/mL) and BMSC (2×10^7/mL) was prepared and fed to the OHC-PEO-CHO solution forming the hydrogels of DN, HA-DN, VEGF-DN and VEGF/HA-DN for 3D co-culture. Each hydrogel was generated in a 48-well plate and transferred to a 24-well plate supplemented with 1 mL of combined medium (DMEM and MSCM) per well. The co-culture hydrogel scaffold was stored in a CO_2 incubator at 37 °C. The cultivation medium was refreshed after 1, 4, 7, 10, and 14 days. Compositions of the groups are listed in Table S1.

The cell-incorporating hydrogel was fixed in 2.5% of glutaraldehyde

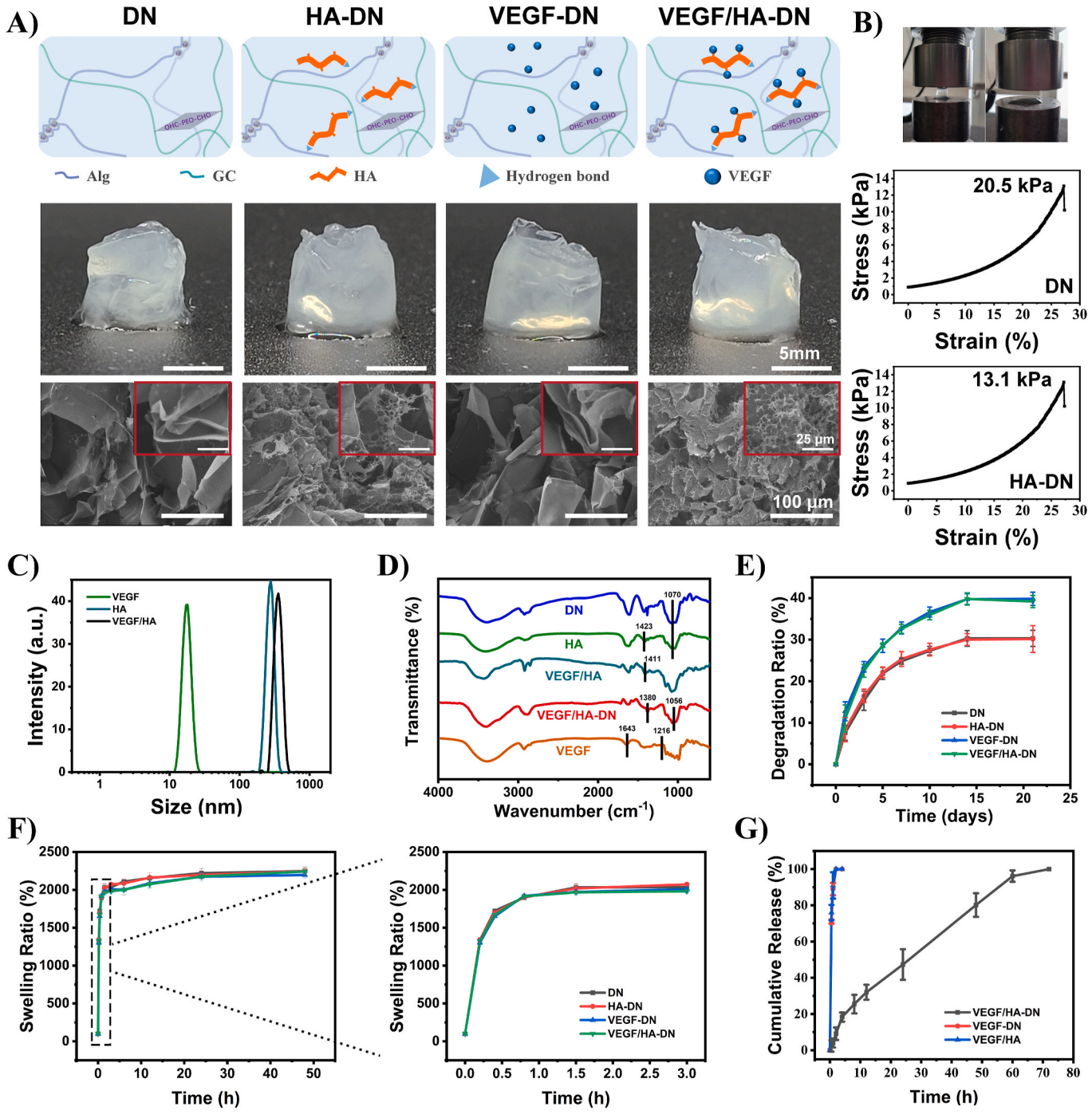

Fig. 1. Performances of the representative hydrogels of DN, HA-DN, VEGF-DN, and VEGF/HA-DN. (A) SEM images of the dried hydrogels. Compared with the hydrogels without HA, pores in the freeze-dried HA-DN and VEGF/HA-DN hydrogels are smaller. (B) The hydrogels before and after compression, and the stress-strain profiles of DN and HA-DN hydrogels. (C) Dynamic light scattering profiles of VEGF, HA, and VEGF/HA complex. (D) FT-IR spectra of the hydrogels of DN, HA, VEGF/HA, VEGF/HA-DN, and pure VEGF. (E) Degradation of the hydrogels within 21 days. The degradation rates at 21 days are 30.3 ± 2.0% for DN, 30.2 ± 3.2% for VEGF-DN, 39.9 ± 1.6% for HA-DN, 39.2 ± 1.5% for VEGF/HA-DN. (F) The swelling ratio of the hydrogels within 48 h. (G) Accumulative VEGF release profiles of VEGF/HA-DN and VEGF-DN hydrogels, and VEGF-HA complex.

for 2 h, rehydrated in gradient ethanol, and prepared by the lyophilized method for SEM observation.

2.4.2. Cell proliferation of 3D EC-BMSC co-culture in the hydrogels in vitro

On days 0, 7, and 14, the co-culture hydrogel scaffold was incubated in 1 mL of CCK-8 reagent and the combined medium (DMEM and MSCM) at a ratio of 1:10. After 4 h, the medium in the well was transferred to a 96-well plate. The absorbance value at 450 nm was recorded on an automatic enzyme-linked immunosorbent assay reader (ELx800, BioTek Instruments, Inc., USA).

2.4.3. Cell differentiation of 3D EC-BMSC co-culture in the hydrogels in vitro

On days 7 and 14, total RNA was extracted from the 3D cultured cells by the RNAeasy™ Animal RNA Extraction Kit (Biotime, Shanghai, China). The RNA was reverse-transcribed to cDNA by using 5 × PrimeScript RT Master Mix (TaKaRa, Japan) under the following conditions: 37 °C for 5 min, 85 °C for 5 s, and 4 °C for 10 min. The cDNA samples were subsequently analyzed by using SYBR Green master rox (Roche Diagnostics Ltd, Mannheim, Germany) and QuantStudio3 Real-Time PCR system (Thermo Fisher Scientific, USA) to measure the expression of cell angiogenesis-related genes (*VEGF-A*, *PECAM1*, and *MMP-9*). The primer sequences are listed in Table S2.

The hydrogel samples were collected after the incubation for 7 and 14 days and immersed in Triton-X (1%) for 30 min to perforate the cell membranes in a confocal dish. After the samples were washed with PBS, they were incubated with sheep serum for 30 min at room temperature. The hydrogel samples were incubated with the primary antibody against CD31 (1:100, Abcam, USA) at 4 °C overnight. The samples were stored at room temperature for 30 min, washed with PBS, and incubated with the proper secondary antibody (1:100, Abcam, USA) for 1 h in darkness. They were soaked in fluorescent mounting medium with 4,6-diamidino-2-phenylindole (DAPI, ZSGB-BIO, China) to stain the nuclei of the cells encapsulated in the hydrogels. The immunofluorescence was observed by TCS-SP8 STED 3X laser confocal microscope (Leica, Germany). The quantitative average optical density (AOD) values and ratio of CD31/nucleus were analyzed by ImageJ 1.54b. The code used to conduct the batch calculation is shown in Fig. S7.

2.5. In vivo observation of 3D EC-BMSC co-culture in the hydrogels

2.5.1. In situ subcutaneous injection of the hydrogels in mice

The animal experiments were approved by the Laboratory Animal Welfare Ethics Branch of the Biomedical Ethics Committee of Peking University (approval number: LA2017049). After passing the quarantine, the experimental animals were adapted to the environment and reared for one week. The mice were randomly divided into 4 groups with 9 mice in each group after labeling. The groups were DN, HA-DN, VEGF-DN, and VEGF/HA-DN hydrogels with EA.hy926 (0.5×10^6/mL) and BMSC (0.5×10^6/mL) encapsulated. The bilateral dorsal skin sites were wiped with 75% alcohol for disinfection. The hydrogel of 0.4 mL was injected subcutaneously by using a dual-syringe kit. The injection points were pressed gently for 5–10 s to allow gelation, and the circular mound-like bulges were observed. At 2, 4 and 6 weeks, 3 mice per group per time point were sacrificed, and the implanted materials and surrounding tissues were separated. The samples were immediately soaked in paraformaldehyde (PFA) (4% w/v) for fixation for 24 h. After dehydration and paraffin embedding of the hydrogels, the sample slices with a thickness of 5 μm were obtained by using a hand-cranked wheeled slicer.

2.5.2. Hematoxylin and eosin (H&E) staining

The sliced specimens were dewaxed, dehydrated, and stained with hematoxylin and eosin. The bioengineered vascular networks of stained slices were observed with an optical microscope (Nikon, Japan). The average number of blood vessels per mm^2 and the average vascular area (mm^2) were counted under 100-fold microscope fields.

2.5.3. Immunohistochemistry (IHC) assay of the sliced specimens

The dewaxing and dehydration steps were the same as those for H&E staining. For antigen retrieval, the slices were soaked in 1 M sodium citrate, heated at 100 °C for 15–20 min, and washed with PBS. Hydrogen peroxide (3% w/v) was used to remove the endogenous peroxidase, and the samples were incubated in 50 μL of sheep serum for 30 min to block nonspecific antigen binding. For primary antibody conjugation, CD31 and α-SMA antibodies (1:50, Abcam, USA) were fed to the slices, which were incubated at 4 °C overnight. After storage at room temperature for 30 min, the slices were washed with PBS. The secondary antibody was conjugated, and diaminobenzidine (DAB) was developed by the mouse IgG two-step detection kit (ZSGB BIO, Beijing, China). After the nuclei were stained with hematoxylin, the slices were sealed with neutral balsam and observed under an optical microscope. The quantitative average optical density values were analyzed by Image J.

2.5.4. Immunofluorescence assay of the sliced specimens

The steps for antigen retrieval and blocking were the same as those for IHC. VEGFR2 and ERK antibodies (1:50, Abcam, USA) were fed to the slices of VEGF/HA-DN at 2, 4, and 6 weeks, and the slices were incubated at 4 °C overnight. CD31 and α-SMA antibodies (1:50, Abcam, USA) were fed to the slices of the four hydrogels at 2 weeks. After storage at room temperature for 30 min, the slices were washed with PBS and incubated with the proper secondary antibody (1:100, Abcam, USA) for 1 h in darkness. They were soaked in fluorescent mounting medium with DAPI to stain the nuclei of the cells within the hydrogels. The immunofluorescence was observed under TCS-SP8 STED 3X laser confocal microscope. The quantitative average optical density values were analyzed by ImageJ.

2.6. Statistical analysis

All statistical analyses were performed in SPSS 25.0 (IBM Corp., Armonk, NY, USA). One-way ANOVA and independent *t*-test were used to detect the statistical differences. The results were presented as mean ± SD. The significance threshold was $p < 0.05$.

3. Results and discussion

3.1. Preparation of the injectable multi-crosslinked DN hydrogels

As illustrated in Scheme 1A, the multi-crosslinked VEGF/HA-DN double-network hydrogel is constructed by crosslinking GC with OHC-PEO-CHO via dynamic covalent benzoic-imine linkage, while the egg-box structure is formed between calcium ion and alginate chains [23,24]. The freeze-dried parental DN and VEGF-DN hydrogels possess large pores after lyophilization. In comparison, the pores within the HA-DN and VEGF/HA-DN hydrogels become smaller (Fig. 1A). This implies that that the inter-chain interaction in the hydrogel is enhanced with HA chains and thus restricts growth of large ice crystals during the freezing process. On the other hand, no benefit on mechanical property of the DN hydrogel is gained by the addition of HA. The maximum compressive stress of the DN hydrogel is high at 20.5 kPa, while the HA-DN hydrogel displays a compressive stress of 13.1 kPa (Fig. 1B). The slight decrease in compressive stress is attributed to the formation of inter-chain crosslinking among the polysaccharide chains and hence the decrease in crosslinking degree of the Alg network and the compactness of the GC/Alg double network [25]. Formation of the calcium alginate egg-box structure is interrupted by the ionic interaction between the carboxyl groups in HA and Alg. Nevertheless, the hydrogels are sufficiently strong to satisfy the requirements in angiogenesis [13].

In order to achieve a stable incorporation of VEGF within the DN gel, HA was selected to form complexation with VEGF via electrostatic interaction. The VEGF/HA complex displays a much larger mean size of 359 nm than the free VEGF (18 nm) or HA coil (276 nm) in aqueous solution (Fig. 1C). Within the GC/Alg network, multi bonds are formed

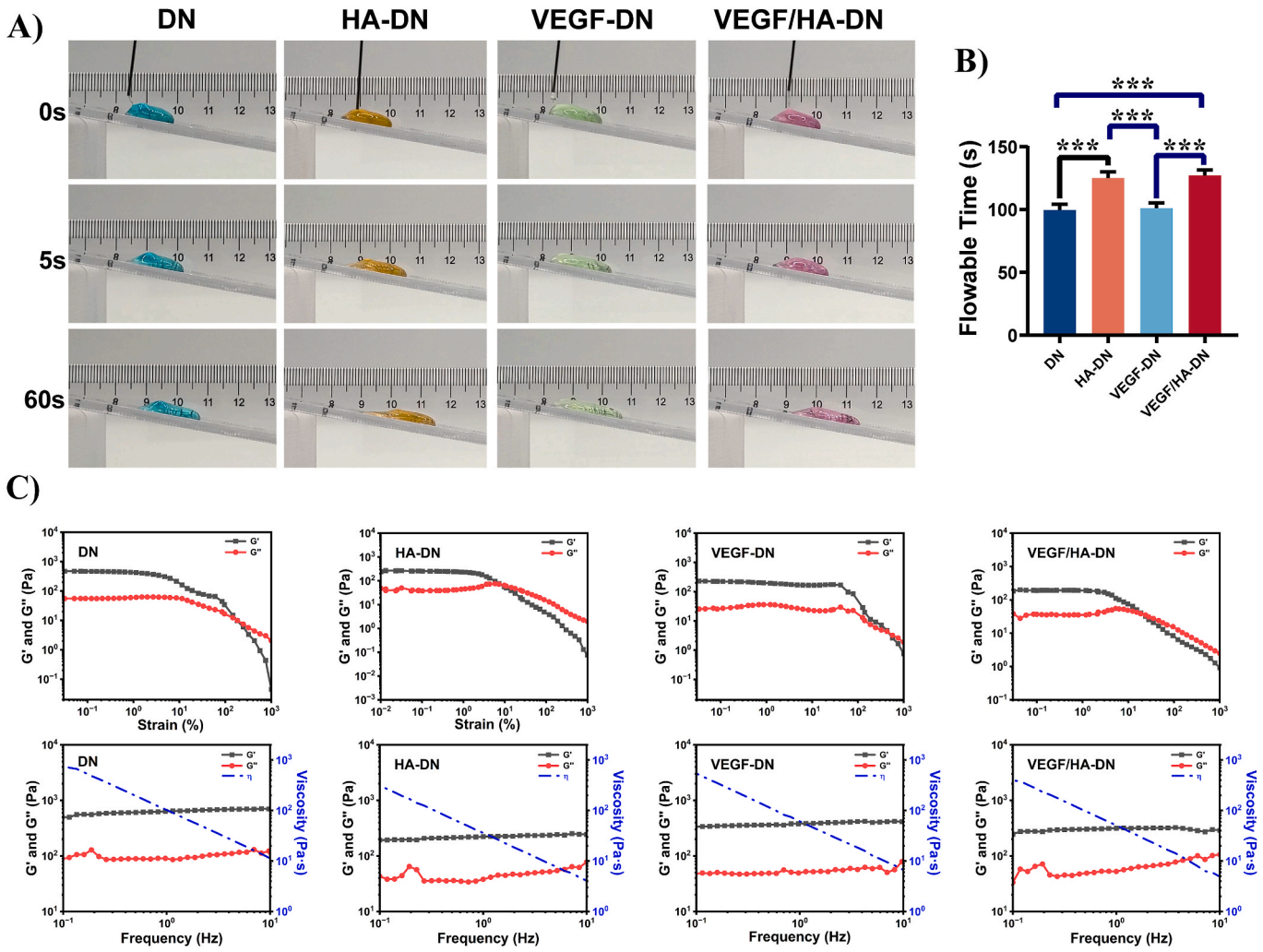

Fig. 2. Flowable time, strain sweeping and frequency sweeping of the hydrogels of DN, HA-DN, VEGF-DN, and VEGF/HA-DN. (A) Experimental model to evaluate flowability of the injectable hydrogels. (B) The flowable times of DN, HA-DN, VEGF-DN, and VEGF/HA-DN measured 60.3 ± 2.1 s, 74.7 ± 1.5 s, 59 ± 2 s, and 75.3 ± 1.5 s. (C) The strain scanning and frequency scanning in a linear viscoelastic region at 37 °C.

between the hydroxyl groups of the polysaccharide of HA, e.g the calcium ion bridging and the hydrogen bonding, in addition to the electrostatic interaction in the VEGF/HA complex. Formation of multi-crosslinks within the VEGF/HA-DN hydrogel is confirmed by FT-IR spectra (Fig. 1D). The absorption peak of carboxyl of HA shifts from 1423 cm^{-1} to 1411 cm^{-1} in the VEGF/HA complex to 1380 cm^{-1} in the freeze-dried VEGF/HA-DN hydrogel. The C–O–C stretching vibration in the DN gel and HA at 1070 cm^{-1} shifts to 1056 cm^{-1} in the VEGF/HA-DN gel.

Degradation rates of HA-DN (39.9 ± 1.6%) and VEGF/HA-DN (39.2 ± 1.5%) hydrogels at 21 days are slightly higher than DN (30.3 ± 2.0%) and VEGF-DN (30.2 ± 3.2%) hydrogels (Fig. 1E). The faster degradation rate of the HA-DN hydrogel is explained by the reduced crosslinking density of the hydrogel, which is consistent with the decreased compressive strength. At 48 h, all the hydrogels demonstrate the similar swelling ratios (Fig. 1F).

In order to effectively promote proliferation of ECs and angiogenesis by VEGF, a sufficient amount of VEGF is required to saturate the VEGFR-2 receptor and polish the influence of VEGF on ECs [26]. For the 3D co-culture system of EC and BMSC *in vitro*, the optimal concentration of VEGF at 50 ng/mL was determined by quantitative real-time PCR to effectively promote vascular differentiation (Figs. S1–S2). An effective release of VEGF from the VEGF/HA and VEGF-DN hydrogels was completed after 1 h (Fig. 1G). The VEGF release from the comparative VEGF/HA-DN hydrogel is much slower with an accumulative release of 5% after 1 h. The complete release was achieved after 72 h (Fig. 1G). The release rate of VEGF from the hydrogels is determined by both the pore size and the interaction of VEGF with the gel matrix [27]. VEGF, composed of two homologous polypeptide chains linked by disulfide bonds, demonstrates an α-helix and β-sheet tertiary structure with a molecular weight of 38–45 kDa [28]. The amide I and amide III bands are assigned at 1643 cm^{-1} and 1216 cm^{-1} in the FT-IR spectrum (Fig. 1D). VEGF with an isoelectric point of 8.5 is positively charged under neutral condition which is capable to combine with negatively charged biomolecules such as HA [29]. The formation of VEGF/HA complex gives rise to a larger hydrodynamic diameter of the peptide and increased binding with the hydrogel matrix. Diffusion of VEGF is thus limited toward the surrounding aqueous phase.

The dynamic nature of the crosslinks renders an easier processability by injection into the desired hydrogels [30]. Both DN and multi-crosslinked DN hydrogels could be smoothly injected through a 26G needle (Fig. 2A). The gelation kinetic is tunable to finish the gelation within 3 min for all the hydrogels. After injection of one hydrogel at a glass slide with a tiling angle of 30°, the hydrogel can flow for some time until cessation. The flow time was thus determined (Fig. 2B). Both hydrogels of HA-DN and VEGF/HA-DN keep moving along a long distance within 60 s. In comparison, the hydrogels of DN and VEGF-DN travel much shorter after 60 s. The two hydrogels of HA-DN and

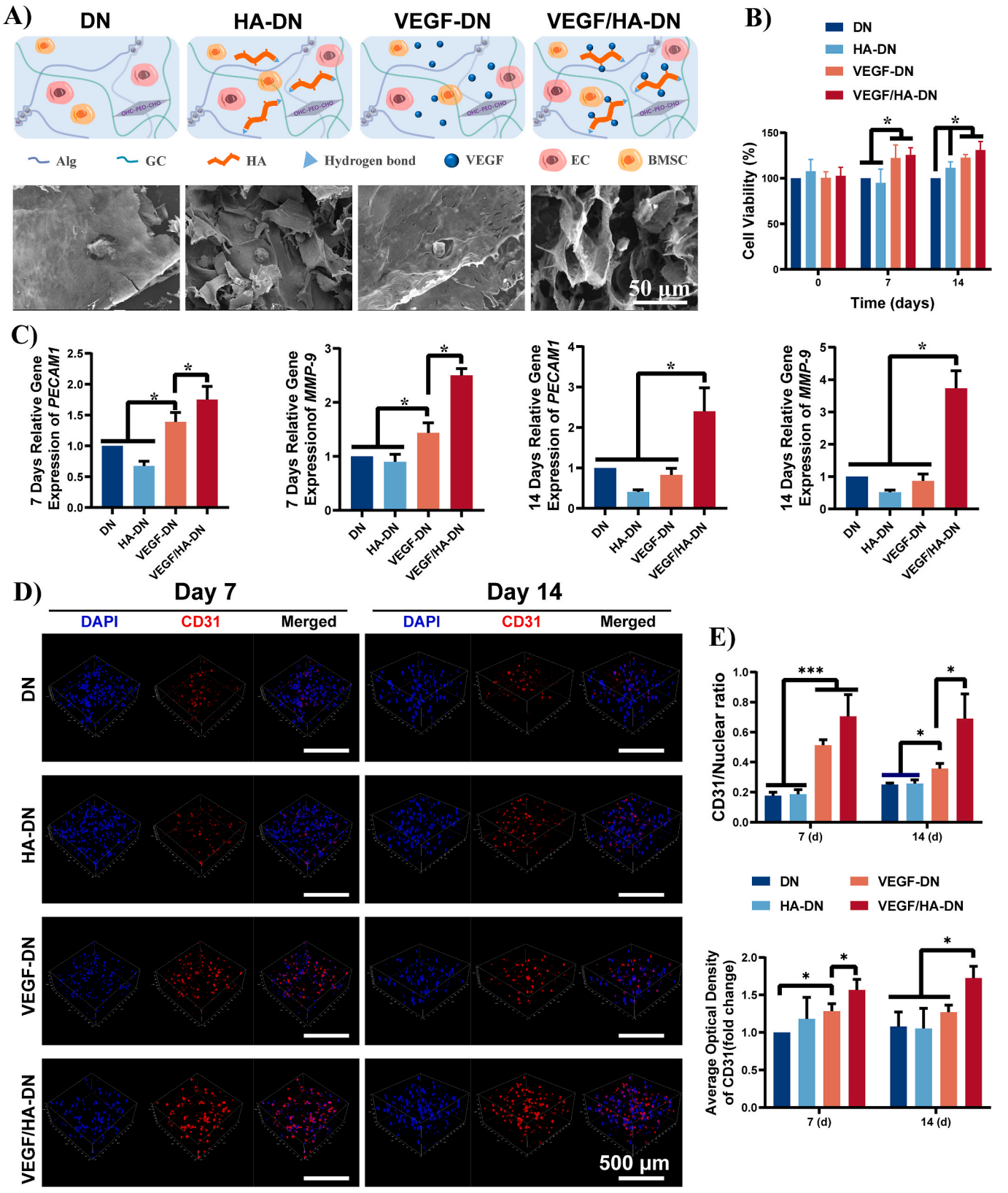

Fig. 3. *In vitro* proliferation and angiogenic differentiation of 3D EC-BMSC co-culture in the hydrogels. (A) Spherical cells are uniformly distributed within the hydrogels. (B) Proliferation activity of 3D co-cultured cells within the hydrogels *in vitro* (*$p < 0.05$). (C) Expression of angiogenesis-related genes (*PECAM1* and *MMP-9*) after 7 and 14 days of culture (*$p < 0.05$). (D) DAPI staining and CD31 in the hydrogels after 7 and 14 days of culture. (E) CD31/nuclei ratio and AOD of CD31 (*$p < 0.05$, ***$p < 0.001$).

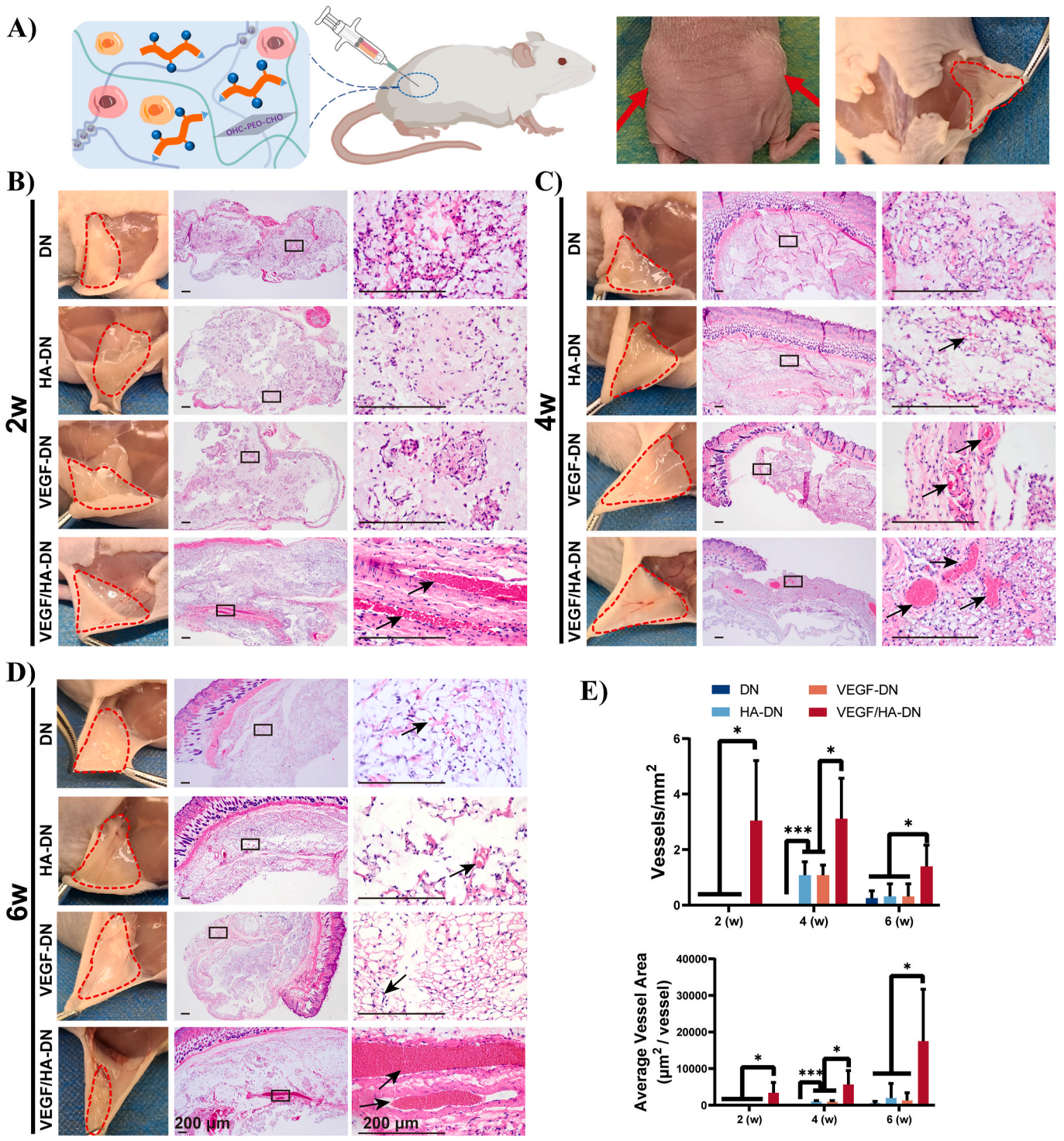

Fig. 4. 3D co-cultured complex of EC-BMSC within the hydrogels to evaluate the angiogenesis performance *in vivo*. (A) Schematic subcutaneous implantation in nude mice. (B–D) H&E staining under a light microscope for 2, 4, and 6 weeks respectively. Blood vessels within the hydrogels are indicated with black arrows. (E) Quantitative analysis of blood vessel formation within the hydrogels (*$p < 0.05$).

VEGF/HA-DN display a longer flow time than DN and VEGF-DN hydrogels. Introduction of HA is conducive to improving processability with a better fluidity and longer gelation time. This is explained by the decreased crosslinking density with the inclusion of HA. As for the measurement of the rheological properties of the hydrogels (Fig. 2C), the linear viscoelastic region (LVR) and yield point of the hydrogels were determined by dynamic strain sweeping at a frequency of 1 Hz. All the hydrogels exhibit the yield performance. The yield points of the HA containing hydrogels (HA-DN and VEGF/HA-DN) are much lower than the HA free hydrogels (DN and VEGF-DN). At a frequency sweeping strain of 0.1%, G′ keeps larger than G'' for the four hydrogels, and a sharp decrease of complex viscosity occurs upon increasing the shear rate implying a significant shear thinning characteristic (Fig. 2C). The shear moduli decrease upon addition of HA, which is explained by a lower crosslinking density and thus easier chain movement under shearing. The highly stain responsive hydrogels should display excellent

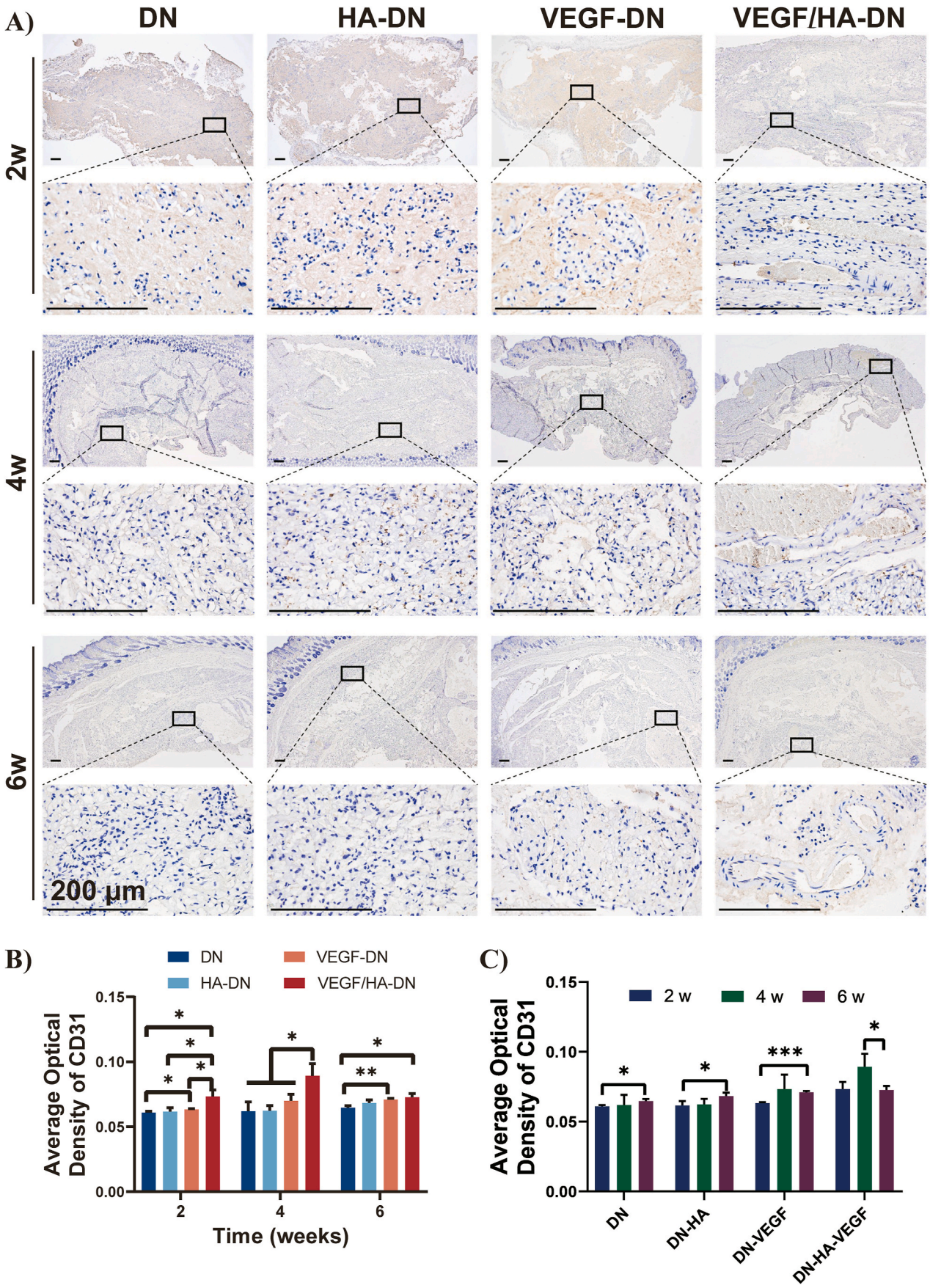

Fig. 5. Expression of the angiogenic protein CD31. (A) Immunohistochemical staining results at 10-fold and 100-fold magnification. (B–C) The average optical density of CD31 in randomly selected visual fields by Image J. The protein expression levels are shown for each time point and group.

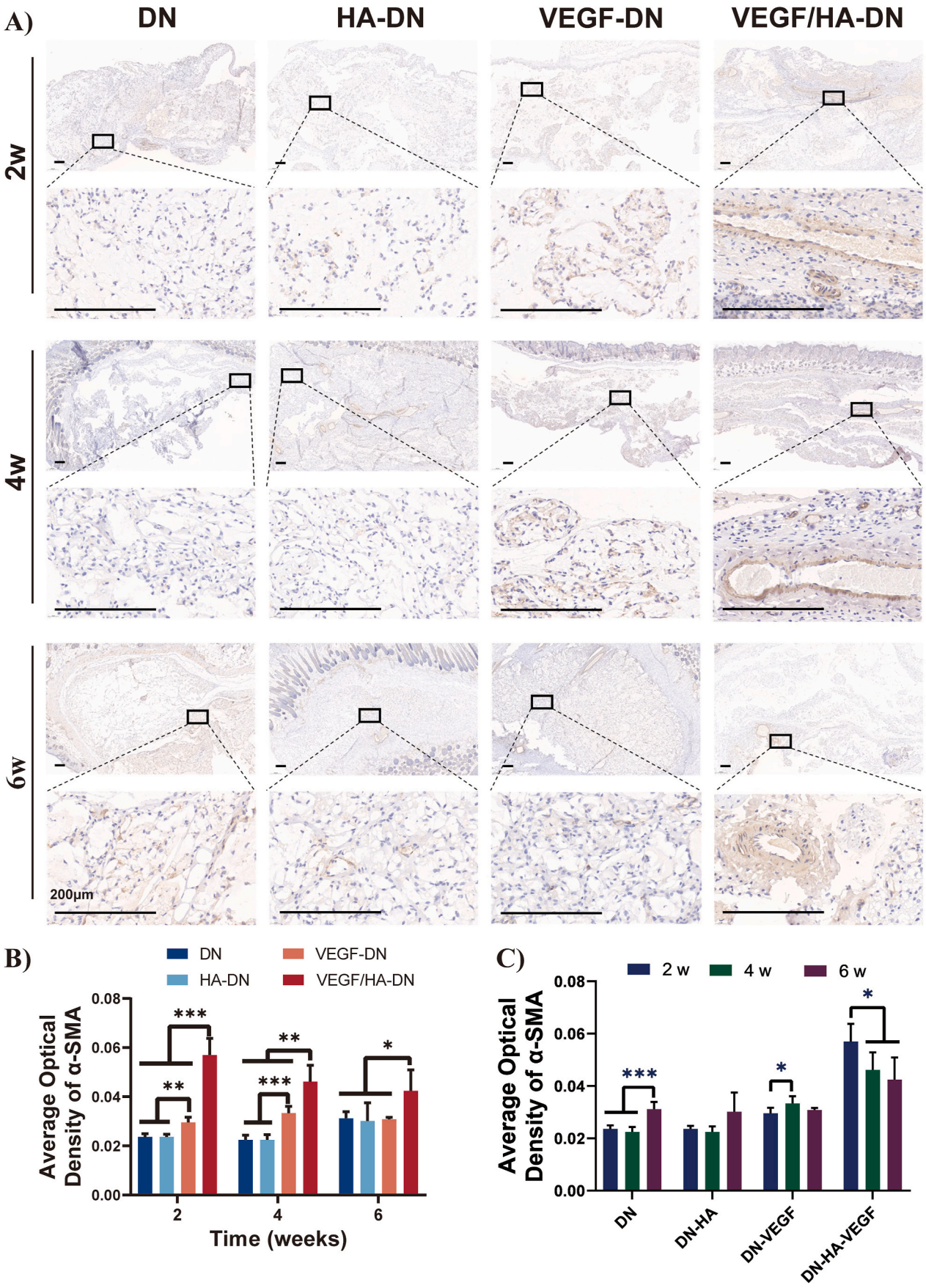

Fig. 6. The expression of α-SMA on pericytes. (A) Immunohistochemical staining results at 10-fold and 100-fold magnification. (B–C) The average optical density of α-SMA in randomly selected visual fields by Image J. The protein expression levels are shown for each time point and group.

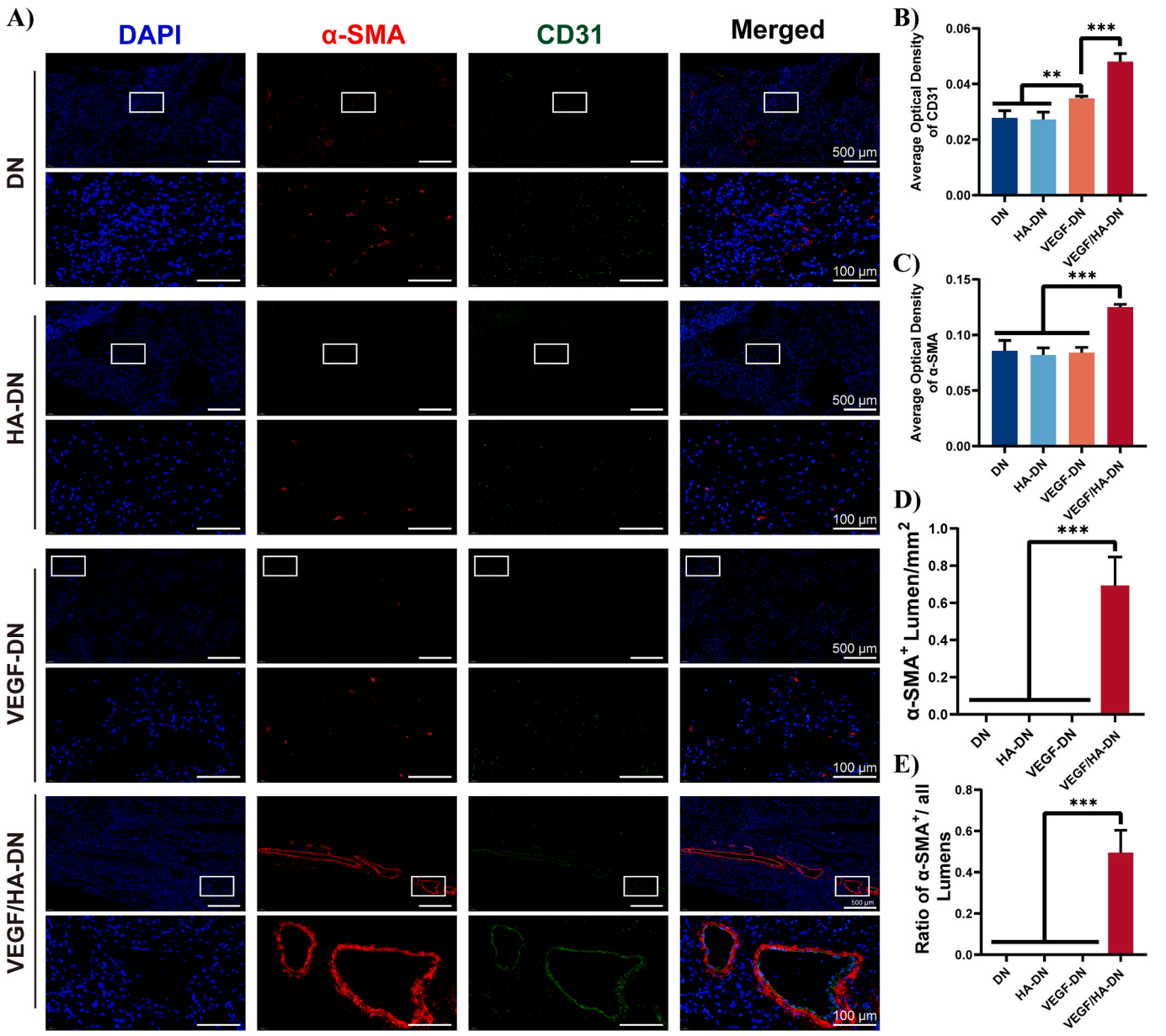

Fig. 7. The results of immunofluorescence double staining of CD31 and α-SMA at 2 weeks. (A) Within the VEGF/HA-DN hydrogel, CD31 is located on the ECs, lining the inner wall of the blood vessels, and α-SMA marks the location of the pericytes. (B–C) AOD values of CD31 and α-SMA within the VEGF/HA-DN hydrogel group (**$p < 0.01$, ***$p < 0.001$). (D–E) The density of lumens formed by CD31 positive cells and the ratio of α-SMA positive lumens to all lumens within the hydrogels.

processing capability by injection.

3.2. *In vitro* observation of 3D EC-BMSC co-culture in the hydrogels

The cells co-cultured within the hydrogels demonstrate spherical contour (Fig. 3A and S3). On day 7, the cell proliferation activities within the VEGF contained hydrogels (VEGF-DN and VEGF/HA-DN) are significantly higher than the other two comparative hydrogels (*$p < 0.05$). For 14 days, the cell proliferation activities within VEGF-DN and VEGF/HA-DN are at the same level ($p > 0.05$). In combination with the previous result of VEGF release, it is shown that the cell proliferation activity by VEGF should be kept continuously for 14 days. The cell proliferation activity within HA-DN becomes slightly higher after 14 days (*$p < 0.05$), although the activity is at a low level (*$p < 0.05$). The result suggests that HA plays a role in promoting cell proliferation (Fig. 3B and S4), which is consistent with the roles in regulation and stimulation of the proliferation of ECs and angiogenesis by HA. In fact, promotion of cell proliferation by HA based oligosaccharide (oHA) has been reported in culturing human umbilical vein endothelial cells (HUVECs) *in vitro* [31]. In the current case, the proliferative effect of HA may be attributed to the in situ production of oHA by degradation during EC proliferation.

In order to characterize formation of blood vessels promoted by the hydrogel, the gene expression levels of *PECAM1* and *MMP-9* were measured by quantitative real-time PCR, whilst CD31 protein was measured by immunofluorescence assay (Fig. 3C–E). On day 7, no significant difference in the expression level of *PECAM1* or *MMP-9* is observed between the two VEGF free hydrogels ($p > 0.05$). In comparison, the angiogenic potential of the VEGF-loaded hydrogels is significantly higher. The angiogenic genes *PECAM1* and *MMP-9* are upregulated to the greatest degree in the VEGF/HA-DN group (*$p < 0.05$). After 14 days, angiogenesis-promoting effect by the VEGF-DN hydrogel starts to decline at the same level as the VEGF free hydrogels ($p > 0.05$). It is noted that the expression of angiogenesis-related genes

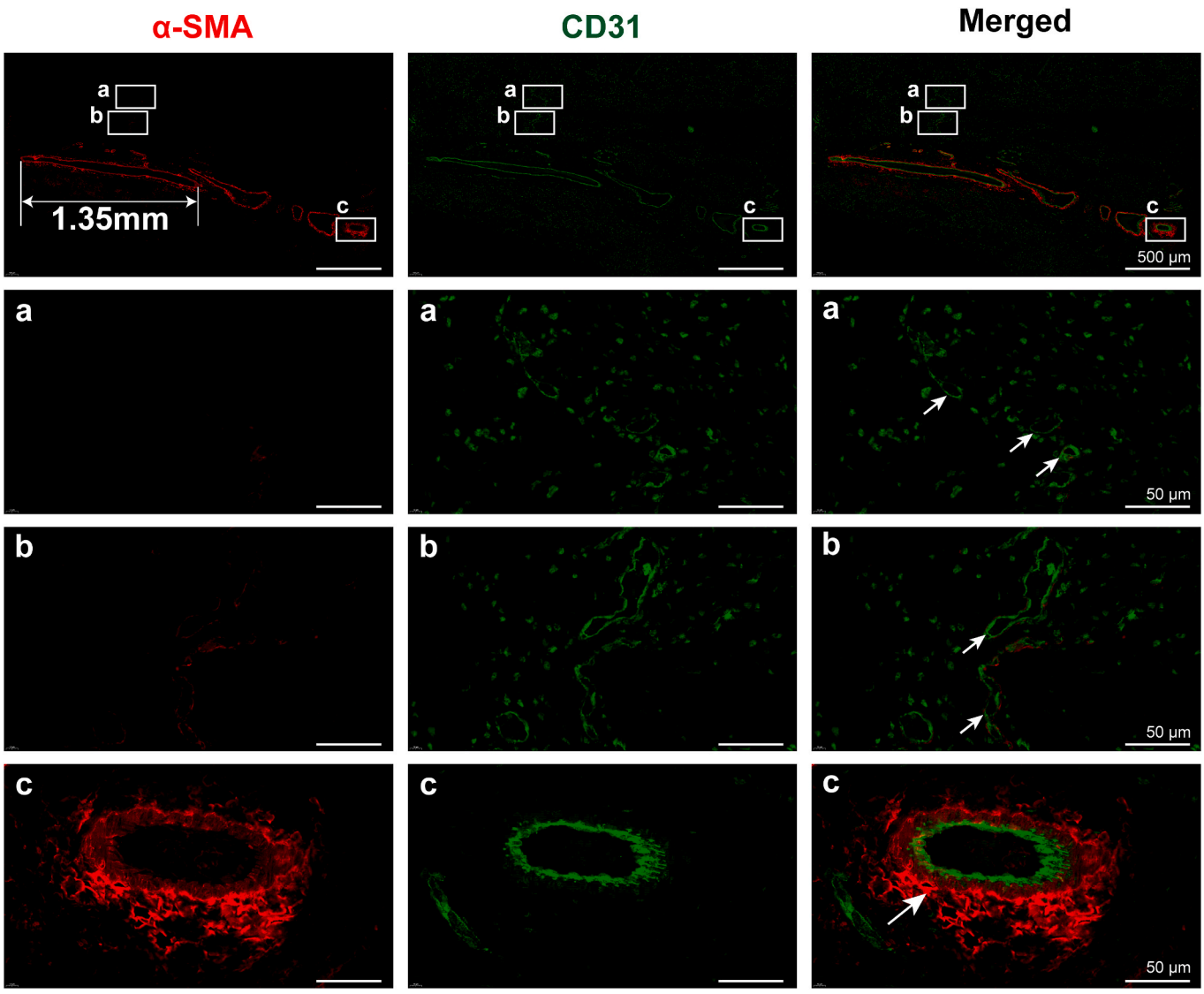

Fig. 8. Vessel structures of different maturity within the VEGF/HA-DN hydrogel at 2 weeks. No α-SMA, a small amount of α-SMA, and a large amount of α-SMA are distributed in Panels a, b, and c, respectively.

*PECAM*1 and *MMP-9* within VEGF/HA-DN is much higher than the other three groups ($^{*}p < 0.05$). PECAM1 (CD31), as a characteristic marker of endothelial cells, is present in most capillaries. CD31 is highly expressed at the ECs surface participating the process of angiogenesis. It is a reliable antigen epitope to characterize angiogenesis. Matrix metalloproteinase-9 (MMP-9) plays an important role in remodeling extracellular matrix and cleaving membrane protein. MMP-9 is capable to induce hydrolysis of extracellular matrix proteins, and support proliferation and migration of endothelial cells. VEGF is responsible to regulate proliferation and survival of ECs thus promoting angiogenesis and increasing vascular permeability [32]. The elevated expression of angiogenesis-related genes in the VEGF/HA-DN group is attributed to a lower release of VEGF than within VEGF-DN. The presence of VEGF is greatly prolonged within the VEGF/HA-DN hydrogel giving rise to a more remarkable expression of angiogenesis-related genes by VEGF. In the immunofluorescence experiment, the AOD value and CD31/nucleus ratio are used to evaluate the expression level of CD31 on the surface of the co-cultured cells. On day 7, both AOD value and CD31/nucleus ratio of the VEGF-DN and VEGF/HA-DN hydrogels are higher than the VEGF free groups (DN and HA-DN). After 14 days, CD31 expression within VEGF/HA-DN is higher than the other three groups ($^{*}p < 0.05$, $^{***}p < 0.001$). The immunofluorescence result is consistent with the gene expression result. This indicates that the effect of VEGF within the VEGF/HA-DN hydrogel on angiogenesis is remarkably prolonged.

ELISA was used to measure concentration of VEGF in the cultivated medium of 3D co-cultured cells *in vitro* (Figs. S5–6). The higher concentration of VEGF in the medium, the lower concentration of VEGF within the hydrogel. Concentration of VEGF within the VEGF/HA-DN hydrogel is lower than within VEGF-DN, implying that the release of VEGF from VEGF/HA-DN is more prolonged. Binding VEGF with HA within the hydrogel is conducive to maintaining a sufficient concentration of VEGF within the hydrogel scaffold for a longer time and thus promoting angiogenesis more effectively.

3.3. *In vivo* angiogenesis of 3D EC-BMSC co-culture in the hydrogels

Subcutaneous injection using dual-syringe kits to form hydrogels is allowed to BALB/c nude mice to investigate the prolonging effect of VEGF on angiogenesis in 3D co-cultured ECs and BMSCs *in vivo* (Fig. 4A). The biocompatibility and *in vivo* degradation of the hydrogels for various times were evaluated. H&E staining, immunohistochemical staining, and immunofluorescence are used to detect the angiogenic differentiation and angiogenesis. BALB/c nude mice born immunodeficient have been widely used as an animal model to evaluate biocompatibility and

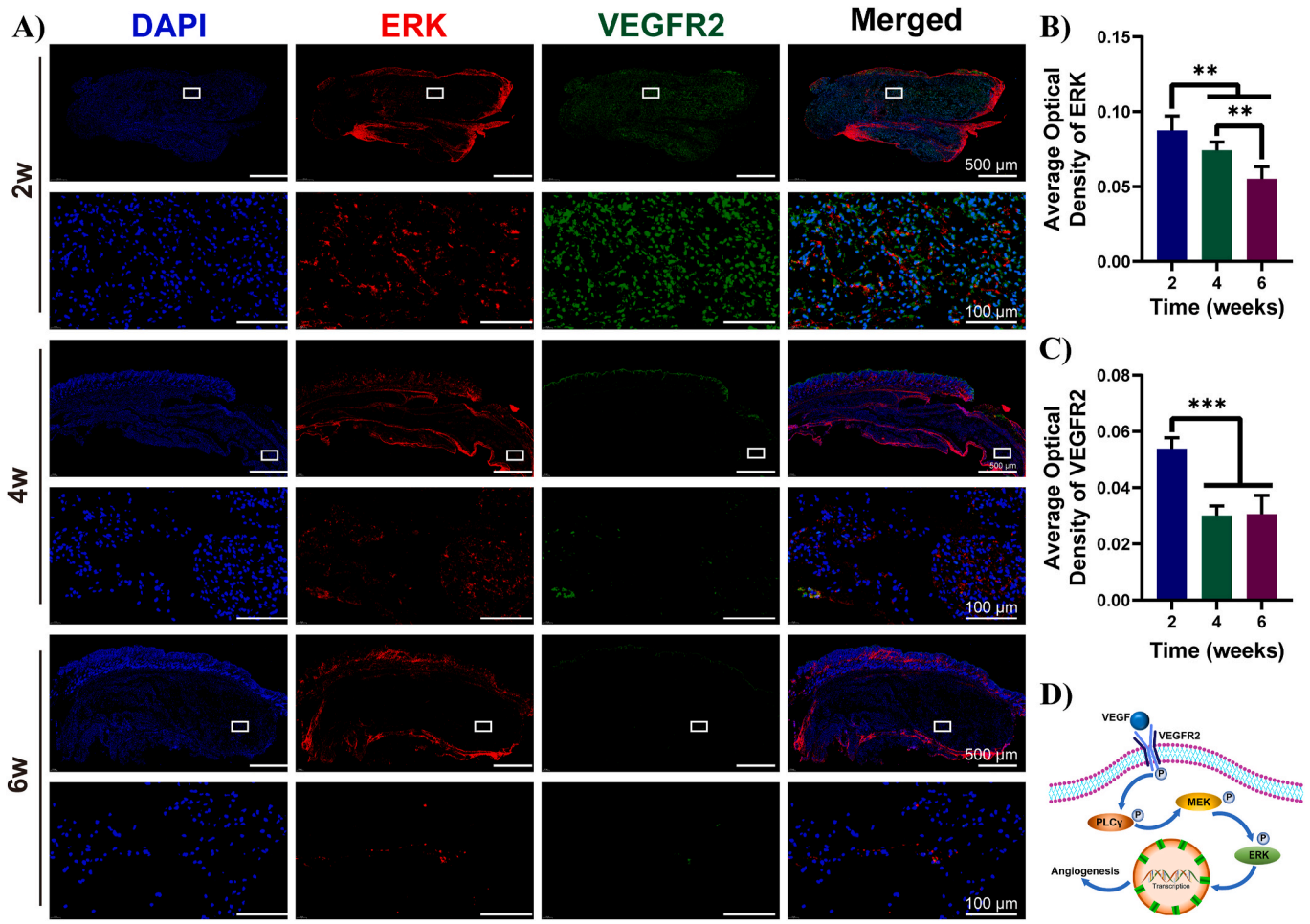

Fig. 9. Hypothesis mechanism of the VEGF/HA-DN hydrogel group in promoting angiogenesis. (A) Immunofluorescence co-staining of VEGFR2 and ERK was conducted at 2, 4 and 6 weeks. (B–C) AOD values of VEGFR2 and ERK at 2, 4 and 6 weeks. (D) Illustrative molecular signaling pathway related with the promotion of angiogenesis.

angiogenesis *in vivo* in tissue engineering. After 6 weeks, all the hydrogels experience a slight degradation. No obvious inflammation is found in the surrounding tissues, indicating that the hydrogels possess a good histocompatibility. At an early stage in tissue engineering at week 2 (Fig. 4B–D), vascular formation occurs only within the VEGF/HA-DN group, and no blood vessels are visualized to naked eyes within the other three groups. In the H&E staining experiments, functional blood vessels form only in the VEGF/HA-DN hydrogel. The blood vessels contain a high number of erythrocytes in the center of each lumen and layered elastic fibers in each vessel wall. Mature neovascularization proceeds within the VEGF/HA-DN group for at least 6 weeks. No obvious blood vessel formation is found in DN group within 4 weeks. A small number of vessels start to form after 6 weeks which are clumped together forming a vessel-like network. This finding is consistent with previous researches [24]. A small number of vessels form within HA-DN and VEGF-DN groups after 4 weeks, indicating that the angiogenesis is promoted by HA or the residual VEGF within the hydrogel. It is understandable that low molecular weight HA is capable to promote the angiogenesis by HA-mediated motility of CD44 and receptors [33]. It is shown that maintenance of some VEGF within the scaffolds is of great significance for early neovascularization and later vascular maturation and reconstruction. The quantitative statistical results (Fig. 4E) show that blood vessel density is decreased and the average vessel area is increased within the VEGF/HA-DN hydrogel with time. Multiple processes are initiated in the presence of angiogenesis factors including MMP-mediated extracellular matrix degradation, pericyte detachment, endothelial cell migration, proliferation, and formation of new blood vessel buds. Extension of the new buds leads to the formation of a lumen which is fused with an immature plexus, and then either matured (e.g. by recruiting pericytes) or trimmed (e.g. by reducing the flow). Eventually, a functional hierarchical vascular network is established to infuse oxygen and nutrients into the surrounding tissues [34].

The blood vessels go via thriving and remodeling forming a steady blood supply for tissue engineering. CD31 and α-SMA are detected by immunohistochemical staining to characterize the endothelial cells and pericytes, respectively (Fig. 5 and 6). Within 6 weeks, expression levels of CD31 and α-SMA within VEGF/HA-DN are significantly higher than the other hydrogels. The abundance decreases with time which is ascribed to the reduction of vessel density in the hydrogels and cell proliferation during the blood vessel reconstruction. The immunofluorescence double staining results for CD31 and α-SMA in the second week (Fig. 7A) indicate that blood vessels are only found within VEGF/HA-DN. CD31 is located on the ECs lining the inner wall of the blood vessels, while α-SMA marking the location of the pericytes is closely adjacent to the ECs outwardly. Although CD31 and α-SMA are expressed within the other three hydrogels, no blood vessels form. The expression of CD31 and α-SMA is much higher within VEGF/HA-DN with higher AOD values (Fig. 7B–C). Density of lumens formed by CD31 positive cells and the ratio of α-SMA positive lumens to all lumens within the hydrogels are shown in Fig. 7D–E. 50% of the lumens are surrounded by α-SMA. Within the blood vessels, α-SMA appears and accumulates progressively along the maturity (Fig. 8).

ECs as the inner lining cells of the vascular lumen are significant in blood vessels at early vascularization. Generation of stable and mature blood vessels is allowed when pericytes are recruited to encapsulate the vessels from ECs [35]. Pericytes secrete growth factors and are important to stabilize blood vessels. The recruiting of pericytes from the host is extremely slow, and it is difficult to separate pericytes from other cells. Exploration of alternative cells is urgently required to support functional vessel formation in TE. Human bone marrow-derived mesenchymal stem cells (hMSCs) are capable to express vascular smooth muscle markers *in vitro* and differentiate into perivascular cells to stabilize blood vessels *in vivo* [36]. ECs and hMSCs could effectively up-regulate the expression of myocardin through cell-cell contact and form stable and functional blood vessels for 130 days during the *in vivo* co-culture [36]. We employed BMSCs as a source of functional cells which could subsequently differentiate into pericytes thus forming functional vessels toward early perfusion.

VEGFR2 and ERK protein fluorescence double staining were performed for various times (Fig. 9A–C). VEGFR2 and ERK expression was found simultaneously, and their average optical densities decrease with time. This finding is related with the decreased vascular density with time while remodeling vessels, which is consistent with the immunohistochemistry results. During the angiogenesis procedure, the VEGFR2/PLCγ/MEK/ERK signaling pathway provides an effective way to promote angiogenesis during vascular network development [32]. Along with the binding of VEGFR2 with VEGF, receptor proteins are bound to form a dimer to phosphorylate and activate the intracellular tyrosine kinase (Fig. 9D). In this study, the expression level of ERK is positively correlated with that of VEGFR2. Upon the activation of VEGFR2, MEK/ERK is subsequently activated transducing a signal into the nucleus to further promote EC proliferation, differentiation, and migration, thereby inducing the formation of lumen [32].

4. Conclusion

We propose a way to co-culture ECs and BMSCs within an injectable multi-crosslinked DN hydrogel with loading VEGF. Action time of VEGF is prolonged to allow a long-term incubation of the cells. Persistent angiogenic differentiation is achieved within the VEGF/HA-DN hydrogel *in vitro*. Early angiogenesis and functional maturation of vessels are achieved after two weeks by administration of the VEGF/HA-DN hydrogel *in vivo*. New vascular structures with an inner layer of endothelial cells and an outer layer of mature and functional pericytes are found by the activation via VEGF/VEGFR2/ERK signaling. Co-culturing EC-BMSC within VEGF/HA-DN hydrogels is promising to achieve early and enhanced angiogenesis in tissue engineering applications.

CRediT authorship contribution statement

Shuqin Chen and **Bing Han** contributed equally to this work. **Shuqin Chen**: Conceptualization, Methodology, Validation, Formal analysis, Investigation, Writing – original draft, Visualization. **Bing Han**: Conceptualization, Methodology, Validation, Formal analysis, Investigation, Writing – original draft, Visualization. **Yanran Zhao**: Formal analysis, Methodology, Investigation. **Yingying Ren**: Formal analysis, Methodology, Investigation. **Shili Ai**: Methodology, Investigation.

Moran Jin: Methodology, Investigation. **Yilin Song**: Methodology, Investigation. **Xiaozhong Qu**: Conceptualization, Supervision, Funding acquisition, Writing – review & editing. **Xiaoyan Wang**: Conceptualization, Supervision, Funding acquisition, Project administration, Writing – review & editing.

Declaration of competing interest

The authors declare that they have no known competing financial interests or personal relationships that could have appeared to influence the work reported in this paper.

Data availability

Data will be made available on request.

Acknowledgements

This work is supported by the National Natural Science Foundation of China (NO.81771061, 52273062 and 51473169).

Appendix A. Supplementary data

Supplementary data to this article can be found online at https://doi.org/10.1016/j.polymertesting.2023.108109.

References

[1] J.J. Kim, L. Hou, N.F. Huang, Vascularization of three-dimensional engineered tissues for regenerative medicine applications, Acta Biomater. 41 (2016) 17–26, https://doi.org/10.1016/j.actbio.2016.06.001.
[2] C. Li, X. Han, Z. Ma, T. Jie, J. Wang, L. Deng, W. Cui, Engineered customizable microvessels for progressive vascularization in large regenerative implants, Adv. Healthc. Mater. 11 (2022), 2101836, https://doi.org/10.1002/adhm.202101836.
[3] Y. Wang, R.K. Kankala, C. Ou, A. Chen, Z. Yang, Advances in hydrogel-based vascularized tissues for tissue repair and drug screening, Bioact. Mater. 9 (2022) 198–220, https://doi.org/10.1016/j.bioactmat.2021.07.005.
[4] Q. Zhang, Y. Liu, J. Li, J. Wang, C. Liu, Recapitulation of growth factor-enriched microenvironment via BMP receptor activating hydrogel, Bioact. Mater. 20 (2023) 638–650, https://doi.org/10.1016/j.bioactmat.2022.06.012.
[5] L. Cheng, Z. Cai, T. Ye, X. Yu, Z. Chen, Y. Yan, J. Qi, L. Wang, Z. Liu, W. Cui, L. Deng, Injectable polypeptide-protein hydrogels for promoting infected wound healing, Adv. Funct. Mater. 30 (2020), 2001196, https://doi.org/10.1002/adfm.202001196.
[6] Y. Zha, Y. Li, T. Lin, J. Chen, S. Zhang, J. Wang, Progenitor cell-derived exosomes endowed with VEGF plasmids enhance osteogenic induction and vascular remodeling in large segmental bone defects, Theranostics 11 (2020) 397–409, https://doi.org/10.7150/thno.50741.
[7] S.E. Est-Witte, A.L. Farris, S.Y. Tzeng, D.L. Hutton, D.H. Gong, K.G. Calabresi, W. L. Grayson, J.J. Green, Non-viral gene delivery of HIF-1α promotes angiogenesis in human adipose-derived stem cells, Acta Biomater. 113 (2020) 279–288, https://doi.org/10.1016/j.actbio.2020.06.042.
[8] T. Yao, H. Chen, R. Wang, R. Rivero, F. Wang, L. Kessels, S.M. Agten, T. M. Hackeng, T.G.A.M. Wolfs, D. Fan, M.B. Baker, L. Moroni, Thiol-ene conjugation of VEGF peptide to electrospun scaffolds as potential application for angiogenesis, Bioact. Mater. 20 (2023) 306–317, https://doi.org/10.1016/j.bioactmat.2022.05.029.
[9] L. Li, Q. Li, L. Gui, Y. Deng, L. Wang, J. Jiao, Y. Hu, X. Lan, J. Hou, Y. Li, D. Lu, Sequential gastrodin release PU/n-HA composite scaffolds reprogram macrophages for improved osteogenesis and angiogenesis, Bioact. Mater. 19 (2023) 24–37, https://doi.org/10.1016/j.bioactmat.2022.03.037.
[10] X. Yu, X. Wang, D. Li, R. Sheng, Y. Qian, R. Zhu, X. Wang, K. Lin, Mechanically reinforced injectable bioactive nanocomposite hydrogels for in-situ bone regeneration, Chem. Eng. J. 433 (2022), 132799, https://doi.org/10.1016/j.cej.2021.132799.
[11] T.H. Qazi, J. Wu, V.G. Muir, S. Weintraub, S.E. Gullbrand, D. Lee, D. Issadore, J. A. Burdick, Anisotropic rod-shaped particles influence injectable granular hydrogel properties and cell invasion, Adv. Mater. 34 (2022), 2109194, https://doi.org/10.1002/adma.202109194.
[12] Y. Qian, Y. Zheng, J. Jin, X. Wu, K. Xu, M. Dai, Q. Niu, H. Zheng, X. He, J. Shen, Immunoregulation in diabetic wound repair with a photoenhanced glycyrrhizic acid hydrogel scaffold, Adv. Mater. 34 (2022), 2200521, https://doi.org/10.1002/adma.202200521.
[13] Y.C. Chen, R.Z. Lin, H. Qi, Y. Yang, H. Bae, J.M. Melero-Martin, A. Khademhosseini, Functional human vascular network generated in photocrosslinkable gelatin methacrylate hydrogels, Adv. Funct. Mater. 22 (2012) 2027–2039, https://doi.org/10.1002/adfm.201101662.
[14] Y. Li, X. Chen, R. Jin, L. Chen, M. Dang, H. Cao, Y. Dong, B. Cai, G. Bai, J. Justin Gooding, S. Liu, D. Zou, Z. Zhang, C. Yang, Injectable hydrogel with MSNs/microRNA-21-5p delivery enables both immunomodification and enhanced angiogenesis for myocardial infarction therapy in pigs, Sci. Adv. 7 (2021), eabd6740, https://doi.org/10.1126/sciadv.abd6740.
[15] A.M. Figueiredo, P. Villacampa, R. Diéguez-Hurtado, J. José Lozano, P. Kobialka, A.R. Cortazar, A. Martinez-Romero, A. Angulo-Urarte, C.A. Franco, M. Claret, A. M. Aransay, R.H. Adams, A. Carracedo, M. Graupera, Phosphoinositide 3-kinase-regulated pericyte maturation governs vascular remodeling, Circulation 142 (2020) 688–704, https://doi.org/10.1161/CIRCULATIONAHA.119.042354.
[16] S.J. Grainger, B. Carrion, J. Ceccarelli, A.J. Putnam, Stromal cell identity influences the in vivo functionality of engineered capillary networks formed by co-delivery of endothelial cells and stromal cells, Tissue Eng. - Part A. 19 (2013) 1209–1222, https://doi.org/10.1089/ten.tea.2012.0281.

[17] J. Liu, Y.J. Chuah, J. Fu, W. Zhu, D.A. Wang, Co-culture of human umbilical vein endothelial cells and human bone marrow stromal cells into a micro-cavitary gelatin-methacrylate hydrogel system to enhance angiogenesis, Mater. Sci. Eng., C 102 (2019) 906–916, https://doi.org/10.1016/j.msec.2019.04.089.
[18] Y. Yan, M. Li, D. Yang, Q. Wang, F. Liang, X. Qu, D. Qiu, Z. Yang, Construction of injectable double-network hydrogels for cell delivery, Biomacromolecules 18 (2017) 2128–2138, https://doi.org/10.1021/acs.biomac.7b00452.
[19] Y. Sun, D. Nan, H. Jin, X. Qu, Recent advances of injectable hydrogels for drug delivery and tissue engineering applications, Polym. Test. 81 (2020), 106283, https://doi.org/10.1016/j.polymertesting.2019.106283.
[20] B. Han, C. Cao, A. Wang, Y. Zhao, M. Jin, Y. Wang, S. Chen, M. Yu, Z. Yang, X. Qu, X. Wang, Injectable double-network hydrogel-based three-dimensional cell culture systems for regenerating dental pulp, ACS Appl. Mater. Interfaces 15 (2023) 7821–7832, https://doi.org/10.1021/acsami.2c20848.
[21] C. Ding, L. Zhao, F. Liu, J. Cheng, J. Gu, S. Dan, C. Liu, X. Qu, Z. Yang, Dually responsive injectable hydrogel prepared by in situ cross-linking of glycol chitosan and benzaldehyde-capped PEO-PPO-PEO, Biomacromolecules 11 (2010) 1043–1051, https://doi.org/10.1021/bm1000179.
[22] F. Zhu, Y. Chen, S. Yang, Q. Wang, F. Liang, X. Qu, Z. Hu, Surface patterned hydrogel film as a flexible scaffold for 2D and 3D cell co-culture, RSC Adv. 6 (2016) 61185–61189, https://doi.org/10.1039/c6ra11249h.
[23] Y. Duan, Y. Zhao, S. Ai, D. Qiu, X. Wang, X. Qu, Z. Yang, Programmable processing toward stiff composite hydrogels, Macromolecules 55 (2022) 7071–7079, https://doi.org/10.1021/acs.macromol.2c00852.
[24] C. Yang, B. Han, C. Cao, D. Yang, X. Qu, X. Wang, An injectable double-network hydrogel for the co-culture of vascular endothelial cells and bone marrow mesenchymal stem cells for simultaneously enhancing vascularization and osteogenesis, J. Mater. Chem. B 6 (2018) 7811–7821, https://doi.org/10.1039/c8tb02244e.
[25] L. Cao, W. Lu, A. Mata, K. Nishinari, Y. Fang, Egg-box model-based gelation of alginate and pectin: a review, Carbohydr. Polym. 242 (2020), 116389, https://doi.org/10.1016/j.carbpol.2020.116389.
[26] J.B. Gurdon, H. Standley, S. Dyson, K. Butler, T. Langon, K. Ryan, F. Stennard, K. Shimizu, A. Zorn, Single cells can sense their position in a morphogen gradient, Development 126 (1999) 5309–5317, https://doi.org/10.1242/dev.126.23.5309.
[27] J.M.D. Legrand, M.M. Martino, Growth factor and cytokine delivery systems for wound healing, Cold Spring Harbor Perspect. Biol. 14 (2022) a041234, https://doi.org/10.1101/cshperspect.a041234.
[28] M. Simons, E. Gordon, L. Claesson-Welsh, Mechanisms and regulation of endothelial VEGF receptor signalling, Nat. Rev. Mol. Cell Biol. 17 (2016) 611–625, https://doi.org/10.1038/nrm.2016.87.
[29] C.R. Silva, P.S. Babo, M. Gulino, L. Costa, J.M. Oliveira, J. Silva-Correia, R.M. A. Domingues, R.L. Reis, M.E. Gomes, Injectable and tunable hyaluronic acid hydrogels releasing chemotactic and angiogenic growth factors for endodontic regeneration, Acta Biomater. 77 (2018) 155–171, https://doi.org/10.1016/j.actbio.2018.07.035.
[30] V.G. Muir, T.H. Qazi, S. Weintraub, B.O. Torres Maldonado, P.E. Arratia, J. A. Burdick, Sticking together: injectable granular hydrogels with increased functionality via dynamic covalent inter-particle crosslinking, Small 18 (2022), 2201115, https://doi.org/10.1002/smll.202201115.
[31] Z. Wei, E. Volkova, M.R. Blatchley, S. Gerecht, Hydrogel vehicles for sequential delivery of protein drugs to promote vascular regeneration, Adv. Drug Deliv. Rev. 149–150 (2019) 95–106, https://doi.org/10.1016/j.addr.2019.08.005.
[32] R.S. Apte, D.S. Chen, N. Ferrara, VEGF in signaling and disease: beyond discovery and development, Cell 176 (2019) 1248–1264, https://doi.org/10.1016/j.cell.2019.01.021.
[33] D. Park, Y. Kim, H. Kim, K. Kim, Y.S. Lee, J. Choe, J.H. Hahn, H. Lee, J. Jeon, C. Choi, Y.M. Kim, D. Jeoung, Hyaluronic acid promotes angiogenesis by inducing RHAMM-TGFβ receptor interaction via CD44-PKCδ, Mol. Cells. 33 (2012) 563–574, https://doi.org/10.1007/s10059-012-2294-1.
[34] K. Bentley, S. Chakravartula, The temporal basis of angiogenesis, Philos. Trans. R. Soc. B Biol. Sci. 372 (2017), 20150522, https://doi.org/10.1098/rstb.2015.0522.
[35] E.E. Crouch, A. Bhaduri, M.G. Andrews, A. Cebrian-Silla, L.N. Diafos, J.O. Birrueta, K. Wedderburn-Pugh, E.J. Valenzuela, N.K. Bennett, U.C. Eze, C. Sandoval-Espinosa, J. Chen, C. Mora, J.M. Ross, C.E. Howard, S. Gonzalez-Granero, J. F. Lozano, M. Vento, M. Haeussler, M.F. Paredes, K. Nakamura, J.M. Garcia-Verdugo, A. Alvarez-Buylla, A.R. Kriegstein, E.J. Huang, Ensembles of endothelial and mural cells promote angiogenesis in prenatal human brain, Cell 185 (2022) 3753–3769, https://doi.org/10.1016/j.cell.2022.09.004.
[36] P. Au, J. Tam, D. Fukumura, R.K. Jain, Bone marrow derived mesenchymal stem cells facilitate engineering of long-lasting functional vasculature, Blood 111 (2008) 4551–4558, https://doi.org/10.1182/blood-2007-10-118273.
[37] U. Uciechowska-Kaczmarzyk, S. Babik, F. Zsila, K.K. Bojarski, T. Beke-Somfai, S. A. Samsonov, Molecular dynamics-based model of VEGF-A and its heparin interactions, J. Mol. Graph. Model. 82 (2018) 157–166, https://doi.org/10.1016/j.jmgm.2018.04.015.